

All-optical quantum information processing via a single-step Rydberg blockade gate

MOHAMMADSADEGH KHAZALI

Institute for Research in Fundamental Sciences (IPM), Tehran 19538-33511, Iran

Department of Physics, University of Tehran, 14395-547, Tehran, Iran

Institute for Quantum Optics and Quantum Information of the Austrian Academy of Sciences, A-6020 Innsbruck, Austria

Abstract: One of the critical elements in the realization of the quantum internet are deterministic two-photon gates. This CZ photonic gate also completes a set of universal gates for all-optical quantum information processing. This article discusses an approach to realize high fidelity CZ photonic gate by storing both control and target photons within an atomic ensemble using non-Rydberg electromagnetically induced transparency (EIT) followed by a fast, single-step Rydberg excitation with global lasers. The proposed scheme operates by relative intensity modulation of two lasers used in Rydberg excitation. Circumventing the conventional π -gap- π schemes, the proposed operation features continuous laser protection of the Rydberg atoms from the environment noise. The complete spatial overlap of stored photons inside the blockade radius optimizes the optical depth and simplifies the experiment. The coherent operation here is performed in the region that was dissipative in the previous Rydberg EIT schemes. Encountering the main imperfection sources, i.e. the spontaneous emission of the Rydberg and intermediate levels, population rotation errors, Doppler broadening of the transition lines, storage/retrieval efficiency, and atomic thermal motion induced decoherence, this article concludes that with realistic experimental parameters 99.7% fidelity is achievable.

© 2023 Optica Publishing Group under the terms of the [Optica Open Access Publishing Agreement](#)

1. Introduction

While the non-interacting features of photons make them an ideal platform for quantum information, the same characteristic deprives two-body deterministic gates. These gates are required for efficient long-distance quantum communication. They are also needed for simple operations in the nodes of quantum internet [1]. In contrast to photons, highly excited Rydberg atoms feature controllable long-range interaction ideal for the implementation of quantum information [2–8] and quantum matters [9–12]. Hence, one approach in making two-qubit photonic gates is to map the quantum state of non-interacting photons to the highly interacting Rydberg atoms [13–23]. This could be realized under the concept of Rydberg electromagnetically induced transparency (EIT), which supports the lossless propagation of single photons in the form of the so-called Rydberg polaritons [23–35]. However, by having two Rydberg polaritons, the influence of Rydberg blockade breaks the underlying EIT, leading to the loss of photons [23, 36].

To circumvent this decoherence source, new ideas are being explored that go beyond this blockade-type nonlinearity in Rydberg-EIT systems and allow for coherent effective polariton interactions. One approach was to change the interaction strength over the storage and gate operation periods [18]. This approach required the Rydberg polaritons to be stored out of the small blockade radius and at the same time be inside the large blockade radius for the gate operation. The competing conditions would affect the high-fidelity operation. Also storing the polaritons in the appropriate place turned out to be challenging. The other approach was to use exchange interaction as the source of conditional phase instead of blockade [17]. In this case, at large optical depths (OD), the operation occurs before the polaritons enter the blockade radius. In a single-lane collision, due to the blockade effect, the optical depth of the medium

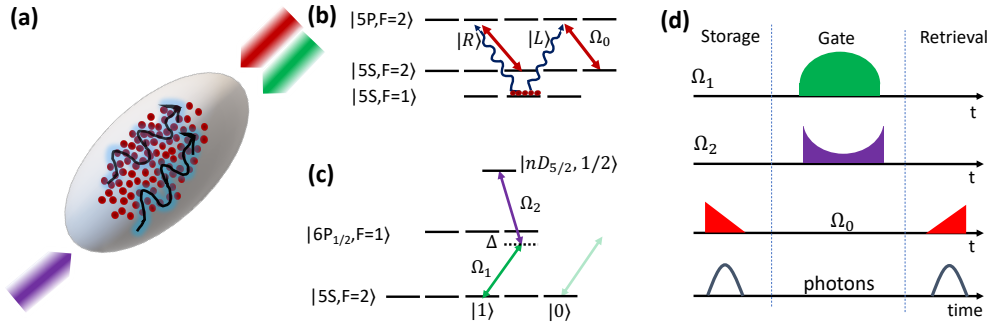


Fig. 1. level scheme. (a) Both control and target photons are stored in the same atomic ensemble that is smaller than the blockade volume. (b) The photon storage is applied via non-Rydberg EIT. The qubit states $|R\rangle$ and $|L\rangle$ would be stored in different ground hyperfine states. (c) Rydberg excitation is derived in a two-photon scheme with global lasers, where the relative strength of two lasers Ω_1/Ω_2 varies over time. Selective excitation of the $|\bar{1}\rangle$ qubit states are governed by using σ^+ circular polarization for Ω_1 laser. (d) The operation timing shows the sequence of applying laser pulses for the photon storage/retrieval and Rydberg gate operation with optimized laser intensity time-varying profiles.

would depend on the two-photon qubit configurations. The conditional optical depth in this case reduces the fidelity. Hence, two rail collision is studied [23] to suppress the loss and conditional OD. However, the competition between the transparency and exchange fidelity still acts as the limiting factor. Even outside the blockade radius, it is argued that the pairwise interaction among Rydberg polaritons could still decouple them from the EIT control field [38]. The other approach studies the storage of photons out of the blockade radius via normal EIT followed by Rydberg excitation [13]. The conditional phase in that scheme is accumulated over time by the space-dependent Rydberg interaction. The accumulated in-homogenous phase, suppresses the fidelity by entangling the spatial and computational basis and reordering the phase matching direction. The common decoherence channel in the aforementioned Rydberg gate schemes was the π -gap- π operation timeline where the excited atoms remained in the Rydberg level over a period of time, unprotected from the laser. This would prevent successful retrieval of the qubit basis [39, 40].

This paper studies a case where storage and interaction are performed in different stages. Both control and target photons are stored in the same medium on top of each other via non-Rydberg EIT. The non-Rydberg EIT [41–43] is the most successful approach in storage and retrieval of single photons in atomic excitations. The absence of blockade among non-Rydberg polaritons provides unconditional uniform storage and retrieval efficiency for all qubit configurations. The perfect overlap of both spin waves optimizes the blockade mechanism and improves the storage region for photons, enhancing the phase-matching direction. Over the gate operation, the new scheme operates by a fast, continuous, and global laser pulse, exciting both spin-waves in $|\bar{1}\rangle$ logical state to the Rydberg level. The relative phase arrangement and retrieval of the logical basis in different qubit configurations are obtained by modulating the relative intensity of two Rydberg exciting lasers combined with the conditional dipolar interaction. This arrangement would close a major decoherence source in conventional π -gap- π Rydberg gate schemes where the operation steps contain a period where excited atoms remain in the sensitive Rydberg level, exposed to the stray fields without laser protection [39, 40]. Considering different decoherence sources, we find the optimum ensemble size and laser arrangement that lead to homogenous conditional phase over the spin-waves, and large OD for efficient storage and retrieval of photons.

The total fidelity of 99.7% is achievable with experimentally realistic parameters.

2. Gate Scheme

The photonic qubits are encoded in the left $|L\rangle$ and right $|R\rangle$ circular polarization components. The *photon storage process* is performed via non-Rydberg EIT [41] in the same medium with the level scheme that is shown in Fig. 1a. The atomic ensemble is initialized in the long-lived hyperfine ground state $|g\rangle = |5S_{1/2}, F = 1, m_f = 0\rangle$. Different polarization components of a photon would be stored in distinguished ground hyperfine states $|0\rangle = |F = 2, m_f = 2\rangle$ and $|1\rangle = |2, 0\rangle$. A single photon forms a single excitation that is delocalized over the atomic ensemble. The spin-wave qubit could be written as

$$C_0|\bar{0}\rangle + C_1|\bar{1}\rangle = 1/\sqrt{N} \sum_i (C_0(\mathbf{x}_i)e^{i\mathbf{k}\cdot\mathbf{x}_i}\sigma_{0g}^{(i)} + C_1(\mathbf{x}_i)e^{i\mathbf{k}\cdot\mathbf{x}_i}\sigma_{1g}^{(i)})|G\rangle \quad (1)$$

where $\sigma_{lm}^{(i)} = |l\rangle\langle m|$ is the transition operator of the i^{th} atom, the overline indicates the delocalized atomic excitation, \mathbf{k} is the spin-wave's wave-vector, \mathbf{x}_i is the position of the i^{th} atom, $|G\rangle$ denotes the state with all atoms in $|g\rangle$, and N being the number of atoms in the ensemble. The spatial profile of the collective excitations is considered in $C_{\{0/1\}}(\mathbf{x}_i)$. Their shape is determined through the storage process and the shape of the input pulses.

The *gate operation* is performed by exciting the $|\bar{1}\rangle$ state of control and target to the Rydberg level via a global pulse. The Rydberg excitation is applied by two-photon excitation with Ω_1 and Ω_2 Rabi frequencies that are red detuned from the $|5P_{1/2}, F = m_f = 1\rangle$ intermediate state by Δ and tuned to $|nD_{5/2}, 1/2\rangle$ Rydberg state, see Fig. 1c. The σ^+ polarization of Ω_1 laser would only excite the $|1\rangle = |F = 2, m_f = 0\rangle$ electronic state to the Rydberg level due to the selection rules, leaving the $|0\rangle$ state unchanged. The effective gate Hamiltonian acting on the two spin-waves is

$$H = \sum_i \left[\left(\frac{\Omega_1(t)}{2} \sigma_{1p}^{(i)} + h.c. \right) + \frac{\Omega_2(t)}{2} \sigma_{rp}^{(i)} + h.c. \right] + \Delta \sigma_{pp}^{(i)} + \sum_{i < j} V(\mathbf{x}_i - \mathbf{x}_j) \sigma_{rr}^{(i)} \sigma_{rr}^{(j)} \quad (2)$$

where $\sigma_{lm}^{(i)} = |l\rangle\langle m|$ is the transition operator of the i^{th} atom.

To apply the desired phase gate $CZ = 2|\bar{00}\rangle\langle\bar{00}| - \mathbb{I}$ with a single continuous global pulse, there are different dynamic parameters including the two lasers' amplitudes, frequencies, and phases that could be varied over time. Here only the lasers' intensities get modulated for the sake of experimental simplicity. Figure 2 shows a suggestive Gaussian time evolution of the Rabi frequencies that retrieves the computational basis for all qubit configurations with the desired conditional phase arrangement. For the qubit configurations $|\bar{10}\rangle$ and $|01\rangle$ the population rotation would add a phase of $\phi_{01} = \phi_{10}$, see Fig. 2c. To describe the effects of relative laser intensities on the population rotation and acquired phase, a simplified case is discussed in App. A. In the case of $|\bar{11}\rangle$, the presence of both spin waves within the blockade volume prevents double Rydberg excitation. The effective operation would then be in a two-dimensional space of $|\bar{11}\rangle$ and the excited \bar{w} state $|\bar{w}\rangle = (|\bar{1r}\rangle + |\bar{r1}\rangle)/\sqrt{2}$. As a result the system derives with an enhanced Rabi frequency and a modified differential light-shift for the $|\bar{11}\rangle - |\bar{w}\rangle$ transition. Hence the population rotation and acquired phase would be different among distinguished qubit configurations as compared in Fig. 2c,d. To operate the CZ gate, the relative Rabi frequencies $\Omega_1(t)/\Omega_2(t)$ would be varied over the operation to retrieve the qubit basis for all qubit configurations and to obtain the desired phase arrangement $\phi_{11} = 2\phi_{01} - \pi$. Compensating for single qubit phase ϕ_{01} with a ground state light-shift, the desired CZ operation will be obtained, see App. C. Compared to conventional Rydberg blockade gate [44] with separate excitation sequence of the control and target qubits over $4\pi/\Omega_{\text{eff}}$ time, this gate operates at a shorter time interval of $t_{\text{gate}} = 2.451\pi/\Omega_{\text{eff}}$ with $\Omega_{\text{eff}} = \Omega_1\Omega_2/2\Delta$. In contrast to the original proposal [44], the Rydberg population over a

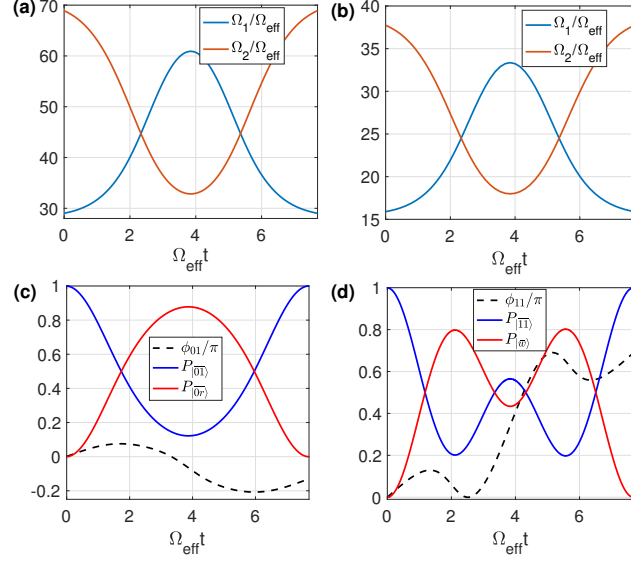


Fig. 2. Simulation of the gate operation (Eq. 2) under a single continuous pulse. Changing the Rabi frequencies $\Omega_{1,2}$ in the form plotted in (a,b) keeps the effective Rabi frequency constant $\Omega_{\text{eff}} = \Delta/1000$ in (a) and $\Omega_{\text{eff}} = \Delta/300$ in (b), and operates the CZ gate over $t_{\text{gate}} = 7.7/\Omega_{\text{eff}}$. The optimized profiles in (a,b) are close to Gaussian profiles with $1/e^2$ width of $2.5/\Omega_{\text{eff}}$. (c) In cases of qubit configurations $|\overline{01}\rangle$ or $|\overline{10}\rangle$, the time evolution of the ground state population and the excited state $|\overline{0r}\rangle$ or $|\overline{r0}\rangle$ are plotted as well as the accumulated phase ϕ_{01} . (d) For the qubit configuration of $|\overline{11}\rangle$, the time evolution of the ground $|\overline{11}\rangle$, $w = (|\overline{1r}\rangle + |\overline{r1}\rangle)/\sqrt{2}$ state, and the accumulated phase ϕ_{11} are plotted.

2π pulse and over the entire gate operation is suppressed by 10% and by two times respectively. This is an important factor as the short lifetime of Rydberg atoms is the main source of infidelity in Rydberg quantum computation.

3. Fidelity & Decoherence sources

The main imperfection sources of the gate operation are caused by spontaneous emissions from the Rydberg and intermediate levels, population rotation errors due to imperfect blockade, Doppler broadening of the transition line, the loss of phase matching due to the thermal motion of atoms, and the inefficiencies of the photon storage in the atomic medium. In Fig. 4,3 the gate operation of Eq. 2 is solved numerically and the gate fidelity is averaged over all input qubit states. The operation is quantified by the phase-sensitive definition of fidelity [45],

$$F = [\text{Tr}(MM^\dagger) + |\text{Tr}(M)|^2]/[n(n+1)] \quad (3)$$

with $M = U_{id}^\dagger U_{gate}$, where U_{id} and U_{gate} , represents ideal and realistic gate operations and $n = 4$ is the dimension of qubit configurations.

Blockade efficiency

Considering the space-dependent interaction over the two delocalized excitations, the *imperfect blockade* in large ensembles results in an inhomogeneous spin-rotation and rotation-induced phase acquisition over the spatial distribution of two spin-waves. In Fig. 3a, the corresponding gate infidelity is quantified by Eq. 3 for the case of localized qubits (diamond signs) as a function of their

distance. The results are then extended to the case of two delocalized qubits in the form of spin-waves (circle/star signs) stored on top of each other. Here a 3-dimensional Gaussian $|C_1(\mathbf{x})|^2 = \exp(-2x_{\parallel}^2/w_{\parallel}^2) \exp(-2\mathbf{x}_{\perp}^2/w_{\perp}^2)$ or super-Gaussian $|C_1(\mathbf{x})|^2 = \exp(-2x_{\parallel}^{10}/w_{\parallel}^{10}) \exp(-2\mathbf{x}_{\perp}^{10}/w_{\perp}^{10})$ profiles are considered, with x_{\parallel} and x_{\perp} being the position vectors along and perpendicular to the lasers' propagation direction. The gate's infidelity is plotted in Fig. 3a as a function of the spin-waves' diameter $D = 2w$ at $1/e^2$ maximum. Considering the anisotropic van der Waals interaction, the same scaling with respect to blockade radius is considered in all directions $D/R_b = D_{\parallel}/R_{b_{\parallel}} = D_{\perp}/R_{b_{\perp}}$. Focusing the incoming photons with super-Gaussian profile to $D = 0.8R_b$ diameter ensures perfect operation with minor gate error of 10^{-3} .

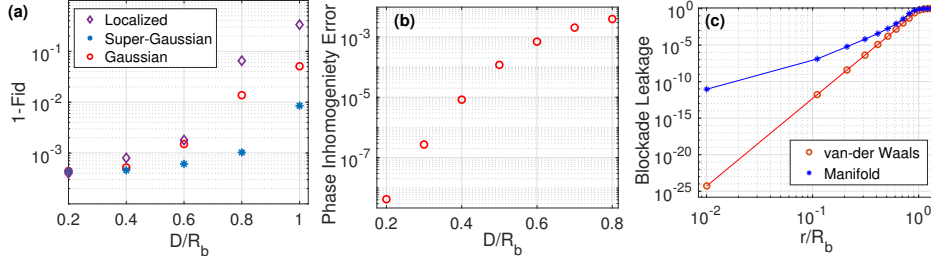


Fig. 3. Blockade imperfection. (a) Gate infidelity caused by an imperfect blockade between two localized atoms (diamond signs) is plotted as a function of interatomic distance D relative to blockade radius. In the case of delocalized excitations, overlapping spin-waves with Gaussian (Circle sign) or Super-Gaussian (star signs) profiles are considered, see the text. The gate's infidelity is plotted as a function of the spin-waves' diameter $D = 2w$ at $1/e^2$ maximum. (b) The population leakage could impose an interaction-induced inhomogeneous phase over the spin-waves. Corresponding gate error is quantified as a function of spin-waves diameter normalized by blockade radius. (c) The validity of van-der Waals interaction applied in (a,b) is investigated. Here the maximum blockade leakage over a 2π rotation is quantified under a more realistic case where the targeted Rydberg pairs are dipole coupled to 1100 other neighbouring pairs (star signs). Compared to the simplified van-der Waals assumption (circle signs) the main deviation occurs at small interatomic distances where the strong couplings deviate the manifold's dynamics from the perturbative regime. For the desired case $0.6 < D/R_b < 0.8$ the error is determined by the double-excitation leakages that are separated far apart and hence the van-der Waals model gives a correct estimate of the gate's operation.

Blockade leakage could also cause an interaction-induced inhomogeneous phase. The phase acquired by each two interacting atoms i and j would be $\phi_{ij} = \int P_{rr}(\mathbf{x}_{ij})V(\mathbf{x}_{ij})dt$ where $V(\mathbf{x}_{ij})$ is the distance dependent van der Waals interaction with $\mathbf{x}_{ij} = \mathbf{x}_i - \mathbf{x}_j$ and $P_{rr}(\mathbf{x}_{ij})$ is the double-excitation leakage probability. The inhomogeneous phase suppresses the fidelity of $|1_c 1_t\rangle$ state by

$$E_{\text{IHPH}} = 1 - \left| \sum_{i,j} |C_1(\mathbf{x}_i)|^2 |C_1(\mathbf{x}_j)|^2 e^{-i\phi_{ij}} \right|^2. \quad (4)$$

The corresponding gate error averaged over qubit configurations is plotted as a function of spin-waves' diameter $D = 2w$ relative to the blockade radius in Fig. 3b. In terms of phase matching, since the leakage predominantly occurs at the edges of the spin-waves, this interaction-induced phase acts as a self-focusing term and hence does not increase photon loss.

While in the above discussion, a simplified van-der Waals interaction is considered, a more realistic case must encounter a huge manifold of dipole-coupled Rydberg pairs. This simplification is justified here by investigating the blockade efficiency under the two models. Figure 3c considers a manifold of 1100 strongly coupled Rydberg pairs with principal and angular quantum numbers

being in the range of $n \in [98 - 102]$, $l \in [0 - 4]$. The maximum blockade leakage over a 2π pulse is plotted for the interatomic orientation parallel with laser fields. The simulation is performed in two atom basis under the Hamiltonian

$$H = \Omega/\sqrt{2}(|gg\rangle\langle r_0g^+| + h.c.) + \Omega/\sqrt{2}(|r_0g^+\rangle\langle r_0r_0| + h.c.) \quad (5)$$

$$+ \sum_{i,j,k,l} \frac{C_{3ij,kl}(\theta)}{R^3} (|r_l r_k\rangle\langle r_i r_j| + h.c.) + \sum_{i,j} \delta_{ij} |r_i r_j\rangle\langle r_i r_j|$$

where the first line excites double Rydberg excitation via the intermediate symmetric state $|r_0g^+\rangle = (|r_0g\rangle + |gr_0\rangle)/\sqrt{2}$. The dipolar interaction $C_{3ij,kl}(\theta)/R^3$ mixes a manifold of Rydberg pairs $|r_i r_j\rangle$ that are detuned in energy from the initial targeted pair $|r_0r_0\rangle = |100D_{5/2}, 1/2; 100D_{5/2}, 1/2\rangle$ by δ_{ij} . While at large inter-atomic distances the result replicates the van-der Waals estimation $V \propto R^{-6}$, at small interatomic distances the strong couplings deviate the manifold's dynamics from the perturbative regime. In quantifying the gate's operation on delocalized excitations in Fig. 3a,b the dominant errors are caused by the excitations that are far apart and hence the van-der Waals model gives a correct estimate of gate's operation for the interest range of spin-waves' size with $0.6 < D/R_b < 0.8$. Finally, at ultra-short distances in the presence of the strong level mixing, the blockade would be preserved due to the diluteness of the optically accessible Rydberg pairs in the manifolds [47]. This has also been proved by blockade experiments in dense atomic ensembles [48–51].

Other imperfection sources

The Doppler shift experienced by atoms moving with thermal velocity v is $\delta_D = \mathbf{v} \cdot \mathbf{k}$ with $\mathbf{k} = \mathbf{k}_1 - \mathbf{k}_2$ being the effective wave-vector of the laser excitation. Hence, a *Doppler broadening* would be experienced by an ensemble with Maxwell velocity distribution $P_v(v) = \sqrt{m/2\pi KT} \exp(-mv^2/2KT)$, where m , K , and T are the atomic mass, Boltzmann constant, and the ensemble temperature respectively. In an ensemble cooled to $1\mu\text{K}$ ($10\mu\text{K}$), counter-propagating beam configuration with wavelengths 1006 nm and 421.7 nm results in a Gaussian Broadening width of $2\pi \times 19$ kHz ($2\pi \times 61$ kHz). At low Rabi frequencies, this effective random detuning $\delta_D \sigma_{rr}$ applies significant deviation of phase and population that affects the average gate's fidelity quantified by Eq. 3. At strong driving regimes, the effect of Doppler line broadening would be negligible, see Fig. 4a,b. The lower limit of the Doppler broadening in Fig. 4b is due to the large intermediate detuning $\Delta/\Omega_{\text{eff}} = 300$ which is a limiting factor in population rotation. In case of a larger detuning $\Delta/\Omega_{\text{eff}} = 1000$ of Fig. 4a the Doppler error keeps reducing at stronger driving regimes.

The *spontaneous emission* from the Rydberg level $|100D_{5/2}, 1/2\rangle$ ($\tau_r = 343\mu\text{s}$) [46] and the intermediate state $|6P_{1/2}\rangle$ ($\tau_p = 129\text{ns}$) suppresses the gate's fidelity as plotted in Fig. 4. Here the loss is quantified phenomenologically by numerical calculation of the Schrödinger equation associated with the Hamiltonian of Eq. 2. To obtain a pessimistic limit of infidelity the entire scattering is considered as loss. Slower operation in (a) allows larger detuning from the $|p\rangle$ state and hence suppresses the corresponding scattering rate. This error could be further suppressed by using the long-lived intermediate state of $|4D\rangle$. The Rydberg decay could be controlled by suppressing the blackbody radiation induced loss using a cryogenic environment or by exciting higher principal quantum numbers $\tau_r \propto n^3$.

The *thermal motion* of atoms disturbs the phase-matching condition and washes out the spin-waves' coherence. The thermal motion's destructive effects quantify as $\eta_{th} = \frac{1}{(1+(\frac{\tau}{\xi})^2)^2} \exp[\frac{-t^2/\tau^2}{(1+(t/\xi)^2)}]$

[52] where $\tau = \frac{\Lambda}{2\pi v}$ is the de-phasing time scale corresponding to the atomic motion over a spin-wave's wave-length Λ with the thermal speed v , and $\xi = \frac{w}{v}$ is the time scale that an atom moves out of spin-wave's profile width w that is about the same length as blockade radius. For the temperature of $T = 1\mu\text{K}$ and $10\mu\text{K}$ the thermal speed of atoms along one direction

would be $v_{th} = \sqrt{K_b T/m} = 0.01$ and 0.03 m/s with K_b , m being the Boltzmann constant and mass of Rb atoms. Considering the non-Rydberg EIT storage scheme of Fig. 1a with counter-propagating photon and classical field, the spin-wave's wavelength $\Lambda = 10$ cm is much larger than the blockade radius and could be neglected. However considering the Rydberg excited spin-wave $|\bar{r}\rangle = \sum e^{i\mathbf{k}_r \cdot \mathbf{x}_i} |g^1 \dots r^i \dots g^N\rangle$ with $k_r = k_{1006} - k_{421}$, the excitation's wave-length would be $\Lambda = 714$ nm which is much shorter than the blockade radius and acts as the limiting factor. Fig. 4a and 4b quantifies the scale of thermal motion infidelity as a function of the gate speed in an ultra-cold medium with $T = 1$ and $10 \mu\text{K}$. The thermal speed of atoms could be suppressed by further cooling or deploying heavier atoms like Cs. The Rydberg wave-vector could be enhanced to $\Lambda = 4.5 \mu\text{m}$ by using $|5D\rangle$ intermediate state in Cs ensemble.

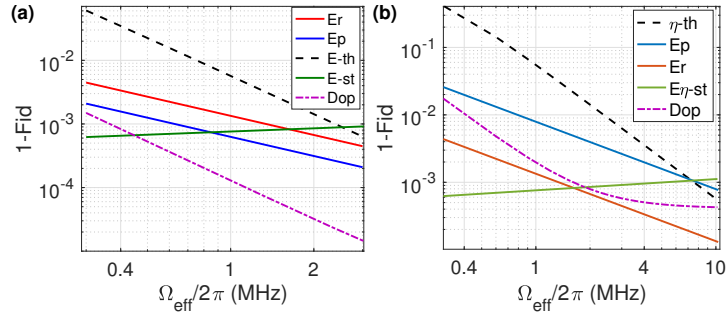


Fig. 4. Gate performance. Error sources are quantified as a function of the gate speed in an ensemble cooled to (a) $T = 1 \mu\text{K}$ and (b) $T = 10 \mu\text{K}$. Quantified error sources include spontaneous emission from the intermediate p state (E_p) and Rydberg levels (E_r). Also, the atomic thermal motion causes the loss of spin-waves' coherence (E_{th}) and raises the population rotation errors due to the Doppler frequency shift (Dop). The storage and retrieval inefficiency E_{st} (under non-Rydberg EIT) is also quantified in an ensemble of length $0.8R_b$ and density of 10^{14}cm^{-3} . Here faster gate operation reduces the blockade radius and hence the medium length, which adversely affecting storage efficiency. Ultra-cold temperature allows slow operation and hence larger detuning from the intermediate state (a) $\Delta/\Omega_{\text{eff}} = 1000$ and (b) 300 which suppresses the loss from the intermediate state. The target Rydberg state is $|100D_{5/2}, 1/2\rangle$ excited via $|6P_{1/2}\rangle$ intermediate states.

The *storage and retrieval efficiency* in the free space EIT is given by $\eta = 1 - 1/OD$ [53] where the optical depth is given by $OD = N\Lambda^2/A$ with N being the number of atoms, Λ the carrier wavelength of the photon, and A the cross-section. In a spherical ensemble with radius R_b we have $OD = 4/3\rho R_b \Lambda^2$. In Fig. 4a,b the storage efficiency is plotted as a function of the gate speed. Higher Rabi frequencies reduce the blockade radius $R_b = (C_6/\Omega_{\text{eff}})^{1/6}$ and hence the optical depth, see Fig. 4a,b. Exciting higher Rydberg principal numbers n could enhance the blockade radius $R_b \propto n^2$ and the optical depth. Cavities could also enhance the optical depth by a factor of F/π where F is the cavity finesse [54].

In an idealized case, we assumed constant spatial and temporal Rabi frequency. In a realistic case, the effects of *inhomogeneity and stability* of exciting beams must be taken into account [59]. In an optical transition $\Omega \propto \sqrt{I}$ with I being the laser intensity, the Rabi frequency fluctuations due to intensity noise is given by $\delta\Omega/\Omega = \delta I/2I$. In a two-photon excitation $\Omega_{\text{eff}} \propto \sqrt{I_1} \sqrt{I_2}$ the Rabi frequency encountering the fluctuations would be given by $\Omega_{\text{eff}}(1 + \delta I_1/2I_1 + \delta I_2/2I_2)$. The noise induced infidelity over a 2π pulse would be $1 - \text{Fid} \approx \pi^2(\delta I_1/2I_1 + \delta I_2/2I_2)^2$. Considering the RMS intensity noise of 0.1% the corresponding infidelity would be 10^{-5} . Regarding the spatial homogeneity, a super-Gaussian transversal profile could be considered for the single-photons (sp) and the classical lasers (L) with HW at $1/e^2$ maximums of $w_L = 1.3R_{b\perp}$ and $w_{sp} = 0.8R_{b\perp}$. In

this arrangement, the gate infidelity of 2×10^{-4} caused by the laser spatial inhomogeneity must be encountered. Using Gaussian profiles for the single-photons ($w_{sp} = 0.8R_{b\perp}$) and driving lasers ($w_L = 2R_{b\perp}$) the infidelity of 6×10^{-4} would contribute to the gate error budgeting.

The Optimum gate speeds discussed in Fig. 4a [4b] are $\Omega_{\text{eff}}/2\pi = 2.3\text{MHz}$ [7MHz]. Considering the super-Gaussian cross-section $I = I_0 e^{-2(\rho/w_\perp)^{10}}$ [56], with the half-width of $w_\perp = 1.3R_{b\perp} = 7.6\mu\text{m}$ [6.3 μm], the required laser powers for the 1006nm laser is 230mW [310mW], see App. B. The transition matrix elements in ^{87}Rb are given by $\langle r \rangle_{5S}^{6P_{3/2}} = 0.528a_0$, $\langle r \rangle_{5S}^{6P_{1/2}} = 0.235a_0$, and $\langle r \rangle_{6P}^{nD} = 0.035 \times (53/n)^{3/2}a_0$. The large dipole transition of 5S-6P allows the same order of Rabi frequency for the 421.7nm transition with a 1mW laser. The mentioned gate speeds provide high-fidelity operations of 99.7% with available experimental parameters.

Conclusion: The proposed photonic gate scheme stores photons in an atomic ensemble and excite them to Rydberg levels in separate steps. The gate operation is carried out via a single continuous global pulse. The desired operation is performed by dynamic modulation of laser intensities applied in the two-photon excitation in the presence of dipolar interaction. This scheme closes major decoherence channels of previous photonic gates and therefore, results to high fidelity operations.

Competing interests- The author declares no conflicts of interest.

Data availability. Data underlying the results presented in this paper are not publicly available at this time but may be obtained from the authors upon reasonable request.

Appendix A

To understand the effects of relative laser intensities on the population rotation and acquired phase, here a simplified case with constant laser parameter is discussed analytically. In the regime of large detuning, $\Delta \gg \Omega_{1,2}$ the intermediate state would be eliminated adiabatically leading to an effective two-level system. Under constant laser parameters, the stored state $|\overline{01}\rangle$ would evolve as

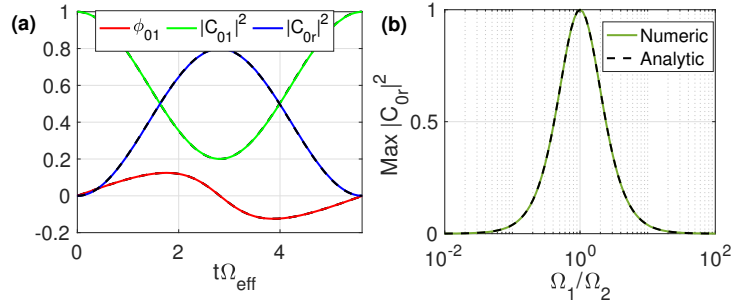


Fig. 5. Justifying the analytic model of Eq. 7 (dashed lines) with the numerical simulation of Eq. 2 (solid lines). (a) Time evolution of the Rydberg excitation of $|\overline{01}\rangle$ qubit state with laser parameters $\Omega_1/\Omega_2 = 0.5$, $\Delta/\Omega_{\text{eff}} = 1000$, $\Omega_{\text{eff}}/2\pi = 10\text{MHz}$. (b) The maximum population of the Rydberg state $|C_{0r}|^2$ could be controlled by adjusting the relative intensity of lasers Ω_1/Ω_2 .

$$\begin{aligned}
|\psi(t)\rangle &= C_{01}(t)|\overline{01}\rangle + C_{0r}(t)|\overline{0r}\rangle \\
C_{01}(t) &= \frac{\Omega_2^2 + \Omega_1^2 e^{it\frac{\Omega_1^2 + \Omega_2^2}{4\Delta}}}{\Omega_1^2 + \Omega_2^2} \\
C_{0r}(t) &= \frac{2\Omega_1\Omega_2}{\Omega_1^2 + \Omega_2^2} e^{it\frac{\Omega_1^2 - \Omega_2^2}{8\Delta}} \sin\left(\frac{\Omega_1^2 + \Omega_2^2}{8\Delta}t\right)
\end{aligned} \tag{6}$$

The population of $|\overline{0r}\rangle$ state and the acquired phase depends on the ratio of Ω_1/Ω_2 as can be seen in Fig. 5.

Appendix B: Achievable Rabi frequencies

Here we discuss the achievable Rabi frequencies for the desired super-Gaussian beams. For the 6P-nD transition strong laser powers above 100W are available in pulsed lasers [58]. For a super-Gaussian cross-section profile, the electric field at the center of the beam E_0 could be obtained from $P = E_0^2/2\eta \int \exp(-2r^{10}/w^{10})2\pi r dr$, where $\eta=377$, $w=7.6\mu\text{m}$, $P=100\text{W}$. The transition matrix elements in ^{87}Rb are given by $\langle r \rangle_{5S}^{6P_{3/2}} = 0.528a_0$, $\langle r \rangle_{5S}^{6P_{1/2}} = 0.235a_0$, and $\langle r \rangle_{6P}^{nD} = 0.035 \times (53/n)^{3/2}a_0$. Hence, the maximum achievable Rabi frequency would be $\Omega_2 = eE_0 \times \langle r \rangle_{6P}^{nD} / \hbar = 2\pi \times 4\text{GHz}$. In the paper, a 20-fold smaller Rabi frequency is considered for optimum operation, resulting in a less demanding experiment.

Appendix C: single-atom phase correction

Over the gate operation with 421.7nm and 1006nm lasers, the former laser applies a differential light shift to the qubit levels. Also, the gate generates ϕ_{01} on each atom at $|1\rangle$ qubit states. These single-atom phases could be compensated after the CZ gate operation by applying a qubit $X(\pi)$ rotation on all atoms and then applying the 421nm pulse (without 1006nm) to correct single qubit phases. The qubits would then be rotated back by a $-X(\pi)$.

References

1. Kimble, H. J. "The quantum internet". *Nature* **453**, 1023 (2008).
2. Saffman, Mark, Thad G. Walker, and Klaus Mølmer. "Quantum information with Rydberg atoms." *Rev. Mod. Phys.* **82**, 2313 (2010).
3. H. Levine, A. Keesling, G. Semeghini, A. Omran, T. T. Wang, S. Ebadi, H. Bernien, M. Greiner, V. Vuletic, H. Pichler, and M. D. Lukin, "Parallel implementation of high-fidelity multiqubit gates with neutral atoms", *Phys. Rev. Lett.* **123**, 170503 (2019).
4. M. Khazali, Klaus Mølmer, "Fast multi-qubit gates via adiabatic evolution in dark state manifolds of Rydberg atoms and superconducting circuits, *Phys. Rev. X* **10**, 021054 (2020).
5. M. Khazali, K. Heshami, C. Simon, "Single-photon source based on Rydberg exciton blockade," *J. Phys. B: Atomic, Molecular and Optical Physics*, **50**(21), 215301 (2017).
6. M. Khazali, "Photonic interface for long-distance entanglement of logical-qubits," *arXiv:2204.08522v1* (2022)
7. M. Khazali, W. Lechner, "Scalable quantum processors empowered by the Fermi scattering of Rydberg electrons." *Communications Physics* **6**, 57 (2023)
8. M. Khazali, "Quantum information and computation with Rydberg atoms", *IJAP* **10**, 19 (2021)
9. M. Khazali, "Discrete-Time Quantum-Walk & Floquet Topological Insulators via Distance-Selective Rydberg-Interaction," *Quantum* **6**, 664 (2022).
10. M. Khazali, "Rydberg Noisy-Dressing and applications in making soliton-molecules and droplet quasi-crystals," *Phys. Rev. Research* **3**, L032033 (2021).
11. M. Khazali, H. W. Lau, A. Humeniuk, C. Simon, "Large Energy Superpositions via Rydberg Dressing," *Phys. Rev. A* **94**, 023408 (2016).
12. M. Khazali, "Subnanometer confinement and bundling of atoms in Rydberg empowered optical lattice", *arXiv:2301.04450* (2023)
13. M. Khazali, K. Heshami, C. Simon, "Photon-photon gate via the interaction between two collective Rydberg excitations," *Phys. Rev. A* **91**, 030301(2015).

14. O'Brien, J. L., Pryde, G. J., White, A. G., Ralph, T. C. & Branning, D. "Demonstration of an all-optical quantum controlled-NOT gate," *Nature* **426**(6964), 264-267 (2003).
15. Hacker, B., Welte, S., Rempe, G. & Ritter, S. "A photon-photon quantum gate based on a single atom in an optical resonator," *Nature* **536**(7615), 193-196 (2016).
16. D Tiarks, S Schmidt-Eberle, T Stolz, G Rempe, S Dürr, "A photon-photon quantum gate based on Rydberg interactions." *Nature Physics* **15** 124-126 (2019).
17. J. D. Thompson, T. L. Nicholson, Q.-Y. Liang, S. H. Cantu, A. V. Venkatramani, S. Choi, I. A. Fedorov, D. Viscor, T. Pohl, M. D. Lukin, and V. Vuletic, "Symmetry-protected collisions between strongly interacting photons," *Nature* **542**(7640), 206-209 (2017).
18. D. Paredes-Barato and C. S. Adams, "All-optical quantum information processing using Rydberg gates," *Phys. Rev. Lett.* **112**, 040501 (2014).
19. YM Hao, GW Lin, K Xia, XM Lin, YP Niu, SQ Gong, "Quantum controlled-phase-flip gate between a flying optical photon and a Rydberg atomic ensemble," *Sci. Rep.* **5**, 10005 (2015).
20. Sumanta Das, Andrey Grankin, Ivan Iakoupov, Etienne Brion, Johannes Borregaard, Rajiv Boddeda, Imam Usmani, Alexei Ourjoumtsev, Philippe Grangier, and Anders S. Sørensen, "Photonic controlled-PHASE gates through Rydberg blockade in optical cavities," *Phys. Rev. A* **93**, 040303 (2016).
21. Wade, A. C. J., Mattioli, M. & Mølmer, K. "Single-atom single-photon coupling facilitated by atomic-ensemble dark-state mechanisms," *Phys. Rev. A* **94**, 053830 (2016).
22. Lahad, O. & Firstenberg, O. "Induced cavities for photonic quantum gates," *Phys. Rev. Lett.* **119**, 113601 (2017).
23. M. Khazali, C. Murry, T. Pohl, "Polariton exchange interactions in multichannel optical networks," *Phys. Rev. Lett.* **123**, 113605 (2019).
24. Friedler, I., Petrosyan, D., Fleischhauer, M. & Kurizki, G. "Long-range interactions and entanglement of slow single-photon pulses." *Phys. Rev. A* **72**, 043803 (2005).
25. Gorshkov, A. V., Otterbach, J., Fleischhauer, M., Pohl, T. & Lukin, M. D., "Photon-photon interactions via Rydberg blockade," *Phys. Rev. Lett.* **107**, 133602 (2011).
26. J. D. Pritchard, D. Maxwell, A. Gauguet, K. J. Weatherill, M. P. A. Jones, and C. S. Adams, "Cooperative atom-light interaction in a blockaded Rydberg ensemble," *Phys. Rev. Lett.* **105**, 193603 (2010).
27. O. Firstenberg, T. Peyronel, Q. Liang, A. V. Gorshkov, M. D. Lukin & V. Vuletic, "Attractive photons in a quantum nonlinear medium," *Nature* **502**(7469), 71-75 (2013).
28. Baur, S., Tiarks, D., Rempe, G. & Dürr, S. "Single-photon switch based on Rydberg blockade," *Phys. Rev. Lett.* **112**, 073901 (2014).
29. Gorniaczyk, H., Tresp, C., Schmidt, J., Fedder, H. & Hofferberth, S. "Single-photon transistor mediated by interstate Rydberg interactions," *Phys. Rev. Lett.* **113**, 053601 (2014).
30. Tiarks, D., Baur, S., Schneider, K., Dürr, S. & Rempe, G. "Single-photon transistor using a Förster resonance," *Phys. Rev. Lett.* **113**, 053602 (2014).
31. Tiarks, D., Schmidt, S., Rempe, G. & Dürr, S. "Optical phase shift created with a single-photon pulse," *Sci. Adv.* **2**, 1600036 (2016).
32. J. Ningyuan, A. Georgakopoulos, A. Ryou, N. Schine, A. Sommer, and J. Simon, "Observation and characterization of cavity Rydberg polaritons," *Phys. Rev. A* **93**, 041802 (2016).
33. H Busche, P Huillery, SW Ball, T Ilieva, M Jones, & C Adams, "Contactless nonlinear optics mediated by long-range Rydberg interactions." *Nature Physics* **13**. 655-658 (2017).
34. Murray, C. R. & Pohl, T. "Coherent photon manipulation in interacting atomic ensembles," *Phys. Rev. X* **7**, 031007 (2017).
35. JD Thompson, TL Nicholson, QY Liang, SH Cantu, A. V. Venkatramani, S. Choi, I. A. Fedorov, D. Viscor, T. Pohl, M. D. Lukin & V. Vuletic, "Symmetry-protected collisions between strongly interacting photons," *Nature* **542**, 206-209 (2017).
36. He, B., Sharypov, A. V., Sheng, J., Simon, C. & Xiao, M. "Two-photon dynamics in coherent Rydberg atomic ensemble," *Phys. Rev. Lett.* **112**, 133606 (2014).
37. Tresp, C., Bienias, P., Weber, S., Gorniaczyk, H., Mirgorodskiy, I., Büchler, H.P. and Hofferberth, S., "Dipolar dephasing of Rydberg D-state polaritons," *Phys. Rev. Lett.*, **115**, 083602 (2015).
38. Tresp, C., Bienias, P., Weber, S., Gorniaczyk, H., Mirgorodskiy, I., Büchler, H.P. and Hofferberth, S. "Dipolar dephasing of Rydberg D-state polaritons," *Phys. Rev. Lett.*, **115**, 083602 (2015).
39. K. M. Maller, M. T. Lichtman, T. Xia, Y. Sun, M. J. Piotrowicz, A. W. Carr, L. Isenhower, and M. Saffman, "Rydberg-blockade controlled-not gate and entanglement in a two-dimensional array of neutral-atom qubits," *Phys. Rev. A* **92**, 022336 (2015).
40. T. M. Graham, M. Kwon, B. Grinkemeyer, Z. Marra, X. Jiang, M. T. Lichtman, Y. Sun, M. Ebert, M. Saffman, "Rydberg mediated entanglement in a two-dimensional neutral atom qubit array," *Phys. Rev. Lett.* **123**, 230501 (2019).
41. M. Fleischhauer, and M. D. Lukin. "Dark-state polaritons in electromagnetically induced transparency." *Phys. Rev. Lett.* **84**(22), 5094 (2000).
42. H Kaviani, M Khazali, R Ghobadi, E Zahedinejad, K Heshami and C Simon, "Quantum storage and retrieval of light by sweeping the atomic frequency," *New J. Phys.* **15**, 085029 (2013) .
43. Y Wang, J Li, S Zhang, K Su, Y Zhou, K Liao, S Du, H Yan & S. L. Zhu , "Efficient quantum memory for

- single-photon polarization qubits", *Nat. Photon.* **13**(5), 346-351 (2019).
44. D. Jaksch, J. I. Cirac, P. Zoller, S. L. Rolston, R. Cote, and M. D. Lukin, "Fast quantum gates for neutral atoms," *Phys. Rev. Lett.* **85**(10), 2208 (2000).
 45. L. H. Pedersen, N. M. Møller, and K. Mølmer, "Fidelity of quantum operations," *Phys. Lett. A* **367**, 47-51 (2007).
 46. I. Beterov, I. Ryabtsev, D. B. Tretyakov, V. M. Entin "Quasiclassical calculations of blackbody-radiation-induced depopulation rates and effective lifetimes of Rydberg n S, n P, and n D alkali-metal atoms with $n \leq 80$," *Phys. Rev. A* **79**, 052504(2009).
 47. M. Khazali, "Progress towards macroscopic spin and mechanical superposition via Rydberg interaction," *Phys. Rev. A* **98**, 043836 (2018)
 48. Ripka, F., Kübler, H., Löw, R. and Pfau, T., "A room-temperature single-photon source based on strongly interacting Rydberg atoms," *Science*, **362**(6413), 446-449 (2018).
 49. Dudin, Y.O. and Kuzmich, A., "Strongly interacting Rydberg excitations of a cold atomic gas," *Science*, **336**(6083), 887-889 (2012).
 50. Ornelas-Huerta, D.P., Craddock, A.N., Goldschmidt, E.A., Hachtel, A.J., Wang, Y., Bienias, P., Gorshkov, A.V., Rolston, S.L. and Porto, J.V., "On-demand indistinguishable single photons from an efficient and pure source based on a Rydberg ensemble," *Optica*, **7**(7), 813-819 (2020).
 51. Shi, S., Xu, B., Zhang, K., Ye, G.S., Xiang, D.S., Liu, Y., Wang, J., Su, D. and Li, L., "High-fidelity photonic quantum logic gate based on near-optimal Rydberg single-photon source," *Nature Comms.* **13**(1), 4454 (2022).
 52. S. D. Jenkins, T. Zhang, T. A. B. Kennedy, "Motional dephasing of atomic clock spin waves in an optical lattice" *J. Phys. B* **45**, 124005 (2012)
 53. A.V. Gorshkov, A. Andre, M.D. Lukin, A.S. Sørensen, "Photon storage in Λ -type optically dense atomic media. II. Free-space model." *Phys. Rev. A* **76**, 033805 (2007).
 54. Y. Jiang, Y. Mei, Y. Zou, Y. Zuo, and S. Du, "Intracavity cold atomic ensemble with high optical depth," *Rev. Sci. Instrum.* **90**, 013105 (2019).
 55. H. Levine, A. Keesling, A. Omran, H. Bernien, S. Schwartz, Alexander S. Zibrov, M. Endres, M. Greiner, V. Vuletic, and M. D. Lukin, "High-fidelity control and entanglement of Rydberg-atom qubits," *Phys. Rev. Lett.* **121**, 123603 (2018).
 56. K. Gillen-Christandl, G.D. Gillen, M.J. Piotrowicz, & M. Saffman, "Comparison of Gaussian and super Gaussian laser beams for addressing atomic qubits." *Applied Physics B* **122**, 1-20 (2016).
 57. Saffman, Mark. "Quantum computing with atomic qubits and Rydberg interactions: progress and challenges." *Journal of Physics B: Atomic, Molecular and Optical Physics* **49**, 202001 (2016).
 58. de Vries, Oliver, Marco Plötner, Florian Christaller, Hao Zhang, Annika Belz, Benjamin Heinrich, Harald Kübler et al. "Highly customized 1010 nm, ns-pulsed Yb-doped fiber amplifier as a key tool for on-demand single-photon generation." *Optics Express* **28**(12) 17362-17373 (2020).
 59. Day, M.L., Low, P.J., White, B., Islam, R. and Senko, C., "Limits on atomic qubit control from laser noise." *npj Quantum Information*, **8**(1), 72 (2022).